THE JOURNAL OF PHYSICAL CHEMISTRY C
A JOURNAL OF THE AMERICAN CHEMICAL SOCIETY

pubs.acs.org/JPCC

Article

A Quasi-Metal–Organic Framework Based on Cobalt for Improved Catalytic Conversion of Aquatic Pollutant 4-Nitrophenol

Minoo Bagheri, Mohammad Yaser Masoomi,* Amparo Forneli, and Hermenegildo García*

Cite This: *J. Phys. Chem. C* 2022, 126, 683–692

Read Online

ACCESS | Metrics & More | Article Recommendations | Supporting Information

ABSTRACT: To generate purposely defects that can increase the catalytic activity, cobalt-based metal–organic framework (MOF) TMU-10 has been subjected to thermal treatment under an air atmosphere at temperatures between 100 and 700 °C. This process causes partial ligand removal, generating structural defects and additional hierarchical porosity in a convenient way. The resulting materials, denoted as quasi-MOFs, were subsequently employed as catalysts for the room-temperature borohydride reduction of 4-nitrophenol (4-NP). The quasi TMU-10 framework obtained at 300 °C (QT-300) exhibits excellent catalytic performance with an apparent rate constant, activity factor, and half-life time of 2.8×10^{-2} s^{-1}, 282 s^{-1} g^{-1}, and 24.8 s, respectively, much better values than those of parent TMU-10. Coexistence of micro and mesopores, coordinatively unsaturated cobalt nodes, tetrahedral Co(II) ions, and Co(III) in QT-300 are responsible for this enhanced activity. Kinetic studies in the range of 25–40 °C varying the 4-NP and BH_4^- concentrations agree with the Langmuir–Hinshelwood model in which both reactants are adsorbed on the catalyst surface. Reduction of 4-NP by the surface-hydrogen species is the rate-determining step.

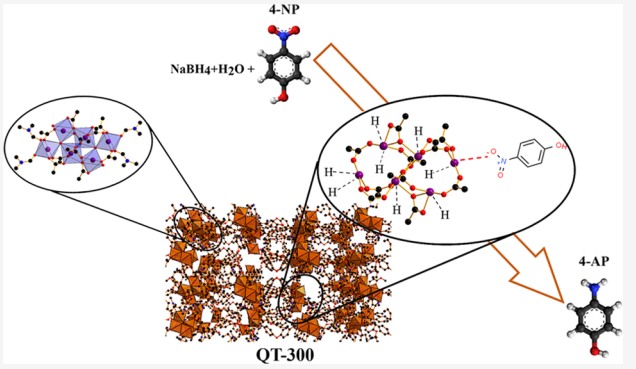

1. INTRODUCTION

Industrial activities can generally result in the generation of significant amounts of harmful substances and pollutants, which are detrimental to the environment and living ecosystems. 4-Nitrophenol (4-NP) is one of the most hazardous and toxic organic contaminants for humans and the environment. 4-NP is generated as a byproduct in a large number of industrial processes; its effects are complicated because of its high solubility and stability in the aquatic environment. Because of its negative impact and toxicity, it is particularly important to remove 4-NP from industrial and agricultural wastewater. At concentrations greater than 20 μg/L, 4-NP is harmful to the central nervous system and could cause blood disorders in humans. Therefore, it is mandatory to develop and improve techniques to deal efficiently with 4-NP and related nitro aromatics in wastewater.[1,2]

One approach to decrease the risks caused by 4-NP is its reduction to 4-aminophenol (4-AP). Reduction of nitro groups to amino is also a general transformation used for the synthesis of numerous analgesic and antipyretic medicines, corrosion inhibitors, dyes, and fuels.[3] Several methods have been applied for this conversion including electrolytic reduction, metal–acid reduction, and catalytic hydrogenation. Electrolytic and metal–acid reduction reactions suffer from some disadvantages. Thus, acidic or alkaline electrochemical reductions suffer from low efficiency, while strong acidic media may be accompanied by weak selectivity. However, catalytic hydrogenation can be considered as a more convenient and advantageous procedure without generating any acidic waste products, while reaching high conversions and selectivity under mild conditions.4 Thus, the heterogeneous catalytic hydrogenation of 4-NP to 4-AP is an important process from the point of view of environmental protection with numerous industrial applications. There have been many studies reporting different catalytic systems such as palladium-graphene nanocomposites[4] and mixed metal oxides.[5,6] However, most catalytic studies for reduction of 4-NP employ noble metals immobilized on different supports such as metal–organic frameworks (MOFs) and spherical polyelectrolyte brushes which are rather costly.[7−13] Some studies have also been performed on non-noble metal cobalt and cobalt oxides with various other catalyst composites.[3,14,15]

MOFs comprising organic ligands and inorganic nodes are considered as a versatile category of porous materials highly suitable to be used as heterogeneous catalysts.[16−18] A high surface area, a large structural variety, designable structure, and

Received: October 3, 2021
Revised: November 18, 2021
Published: December 31, 2021

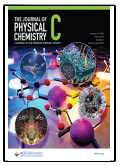

numerous possibilities for metal centers as well as good thermodynamic stability make these materials attractive and ideal candidates for catalytic applications.[16,19−21] As a result, a large number of heterogeneous catalysts based on MOFs and their composites have been reported in the last decade.[22−25] Unfortunately, in many of the MOF structures, the inorganic nodes are completely blocked and saturated by organic linkers that hinder the access to them, leaving no coordination positions available for the binding and activation of substrates. Therefore, a general strategy is needed to increase access to these inorganic nodes and enhance their catalytic activity.

Development of defects in MOFs is well established for enhancement of catalytic activity and also increases porosity. Alongside elimination of the bonded solvent molecules,[26,27] limited removal of ligands via thermal treatment ("*deliganda-tion*") has been used to make the Lewis acid centers.[28−30] Very lately, the term quasi-MOFs (Q-MOFs) has been suggested to illustrate those MOFs subjected to controlled thermal treatment for the generation of defects. Q-MOFs could represent a bridge between highly crystalline MOF materials and metal compounds, and their properties are receiving increasing attention.[29−34] The inherent specific surface area is retained or even enhanced upon partial deligandation along with generation of hierarchical micro and mesopores which facilitates diffusion of substrates to and products from the active centers.[35,36]

We herein report the improved catalytic activity for 4-NP reduction to 4-AP of a cobalt Q-MOF catalyst, obtained from TMU-10. This improved performance of the Q-MOF arises from the creation of super-high density unsaturated metal centers and the simultaneous generation of both micro and mesopores after partial thermal ligand removal treatment. TMU-10 is a suitable MOF to be subjected to deligandation considering its high thermal stability and the existence of hexanuclear secondary building units (SBUs) of cobalt centers.[23] In the adjusted Q-MOF, the porosity and structure of the parent TMU-10 are partially preserved, with the generation of defects that increase diffusion through the material, while creating a coordinatively unsaturated position around the Co ions that exhibit a general catalytic activity in oxidations and reductions. In contrast to most reported metal oxide systems[37] and to obtain an improved catalytic hydride transfer, an effective partial deligandation is a very convenient process to increase a widespread distribution of active metal sites throughout the MOF while avoiding the particle aggregation characteristic of small metal oxide clusters.

So far, MOFs with structural defects in their framework have been evaluated as catalysts in CO oxidation accelerated via oxygen species,[30,38,39] adsorption of CO_2,[31] and benzyl alcohol oxidation.[28] From what we know, this is one of the first reports on the application of Q-MOFs in the catalytic hydride transfer under mild conditions.

TMU10, $[Co_6(oba)_5(OH)_2(H_2O)_2(DMF)_4]_n{\cdot}2DMF$ (H_2oba = 4,4′-oxybisbenzoic acid), has in its structure three crystallographically independent six coordinate Co(II) centers.[23] Herein, it will be described how partial deligandation on TMU-10 can produce a highly active non-noble Q-MOF catalyst, whose activity derives from the presence of coordinatively unsaturated Co Lewis acid sites over the framework, concomitance with micro and mesopores. QTMU-10 has been generated by adjusted thermal behavior in air at diverse temperatures with the aim to partially remove organic ligands to achieve the optimal density and strength of Lewis acid Co nodes tuned to the reaction requirements. The catalytic activity of the obtained Q-MOF drastically modifies with its deligandation temperature. The highest catalytic performance was observed for deligandation treatment at 300 °C; this material performs much better than the parent TMU-10 and that Co_3O_4 nanoparticle. Its reusability and the corresponding kinetic and thermodynamic properties have also been investigated. Our findings demonstrate that QTMU-10 offers a porous structure in which substrate diffusion becomes easier and multisite catalytic centers derived from coordinatively unsaturated metal positions, which are not present in the parent MOF or metal oxide nanoparticles.

2. EXPERIMENTAL SECTION

2.1. Synthesis of TMU-10. TMU-10 powder was synthesized according to the previously reported procedures (see the Supporting Information for more information).[23]

2.2. Synthesis of QT-x. Thermal treatment of TMU-10 was carried out under air at a heating rate of 5 °C min^{-1} up to a final temperature in the range between 100 and 700 °C with a 1 h dwelling time. The samples were marked as QT-x, where "T" and "x" stand for TMU-10 and the final temperature of thermal treatment, respectively. Analysis of the gases evolved upon heating at 300 °C was performed with a gas chromatography (GC)−mass spectrometry (MS) Agilent quadrupolar analyzer.

2.3. Catalytic Activity. The catalytic reduction of 4-NP was followed by UV−vis absorption spectroscopy. Before each run, the solutions were purged with N_2 to remove O_2. For this purpose, 1.0 mg of catalyst was added to 25 mL of fresh 4-NP (0.05 mM) and $NaBH_4$ (10 mM) solutions at room temperature. Then the solutions were stirred vigorously. The conversion of 4-NP was subsequently determined measuring the optical density at λ_{max} = 400 nm at periodic intervals. The catalytic reduction performance was calculated by the following equation:

$$\%\text{Reduction} = (C_i - C_t)/C_i \times 100 \tag{1}$$

where C_i is the initial concentration of 4-NP and C_t is the concentration of 4-NP at any given time.

The kinetics of the reduction reaction can be obtained by eqs 234 as follows:

$$-\frac{dC}{dt} = k_{app}C \tag{2}$$

$$\text{Ln}\left(\frac{C}{C_0}\right) = -k_{app}t \tag{3}$$

$$K = \frac{k_{app}}{m} \tag{4}$$

where k_{app} is the apparent reaction rate, m is the catalyst mass in grams, and K is the activity factor of the catalyst. The activation energy was calculated at 25, 30, 35, and 40 °C. To evaluate catalyst stability, the solid was separated from the mixture by centrifugation and washed several times with methanol and deionized water, then dried at 100 °C under vacuum for 10 h, and finally used in a consecutive reduction reaction. The repeatability and stability tests were carried out five times in the same way as mentioned above.

https://doi.org/10.1021/acs.jpcc.1c08658
J. Phys. Chem. C 2022, 126, 683−692

3. RESULTS AND DISCUSSION

3.1. Characterization. TMU-10, $[Co_6(oba)_5(OH)_2(H_2O)_2(DMF)_4]_n \cdot 2DMF$, is a cobalt-based MOF prepared via refluxing of its precursors as reported in the Experimental Section. In this MOF, hexanuclear SBUs, $Co_6(CO_2)_{10}(O)_2(O)_4$, linked to each other to produce a three-dimensional framework with 32.7% void space per unit cell (Figure 1). Each SBU comprises three crystallographically

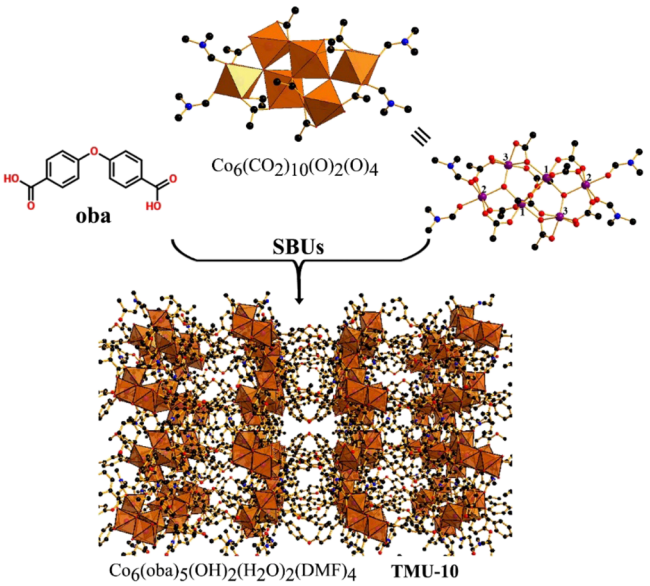

Figure 1. Single-crystal X-ray structure of TMU-10. Color code: O, red; N, blue; C, black; and Co, purple and brick color polyhedra.

independent Co(II) with the coordination spheres that are completed by six oxygen atoms from oba ligands, μ_3-O atoms of OH^- anions, and oxygen atoms of H_2O or DMF molecules (Figure 1).

Various temperatures (i.e., 100, 150, 200, 250, 300, 350, 400, and 700 °C) were chosen for thermal treatment based on the thermogravimetric profile of TMU-10 (Figure S2). These thermal calcinations are required to remove the solvent and a fraction of ligands to generate unsaturated inorganic nodes. The high temperature of 700 °C ensures the complete decomposition of TMU-10. Five coordinate Co(3) centers can be obtained by removal of its bonded water molecule at 150 °C along with removal of two DMF guest molecules from the pores of the framework. Also, by removing the two DMF molecules bounded to Co(2) centers, four coordinated metal centers are formed at 200 °C. Eventually, partial deligandation is achieved at 300 °C by disconnecting two μ_3-O atoms of OH^- anions in the framework which are associated with Co(1), Co(2), and Co(3) with coordination numbers of five, three, and four, respectively. (Figure S3). This proposal was approved by GC−MS in which evolution of H_2O and CO_2 was observed when TMU-10 was heated at 300 °C after prior removal of DMF at 150 °C for 2 h.

Because sample QT-300 was the best performing catalyst (*vide infra*), more detailed characterization was performed for this solid. Investigation of the morphology of TMU-10 and QT-300 samples by field-emission scanning electron microscopy (FESEM) shows that the TMU-10 sample is constituted by nanoparticles (Figure S4a). The thermal treatment to which the QT-300 sample was subjected causes a certain agglomeration of the nanoparticles into larger particles (Figure S4b).

The transformation of the atomic cobalt oxidation state from TMU-10 to QT-300 was evaluated by X-ray photoelectron spectroscopy (XPS) (Figure 2). In the XPS spectrum of TMU-10, the peaks at 780.5 and 796 eV correspond to Co $2p_{3/2}$ and Co $2p_{1/2}$, respectively, which are associated with intense satellite bands centered at 786.3 and 803 eV, all ascribed to octahedral Co(II) atoms.[40] The curve-fitting of QT-300 exhibits four new peaks at 779.6, 782.9, 789, and 804.5 eV which are associated with the Co(III) $2p_{3/2}$ main peak, Co(II) in tetrahedral sites, and two shake-up satellites for Co(III), respectively.[41,42] These results approve that after partial deligandation a fraction of Co(II) centers is altered to Co(III) as well as the formation of tetrahedral Co(II) sites.

Powder X-ray diffraction (PXRD) of TMU-10 at different temperatures indicates that the crystal structure is preserved up to 300 °C with expansion of the diffraction peaks around 6°−7° because of partial deligandation of TMU-10 (Figure 3). A high degree of structural destruction occurs upon increasing the temperature to 350 °C, which is shown by considerable reduction in the intensity of characteristic peaks of TMU-10. Ultimately, TMU-10 is completely converted to Co_3O_4 at 400 °C determined by disappearance of corresponding peaks of TMU-10 and appearance of diffraction peaks of Co_3O_4 (JCPDS No. 42-1467). Nevertheless, a sample QT-700 calcined at even higher temperature (700 °C) and correspond-

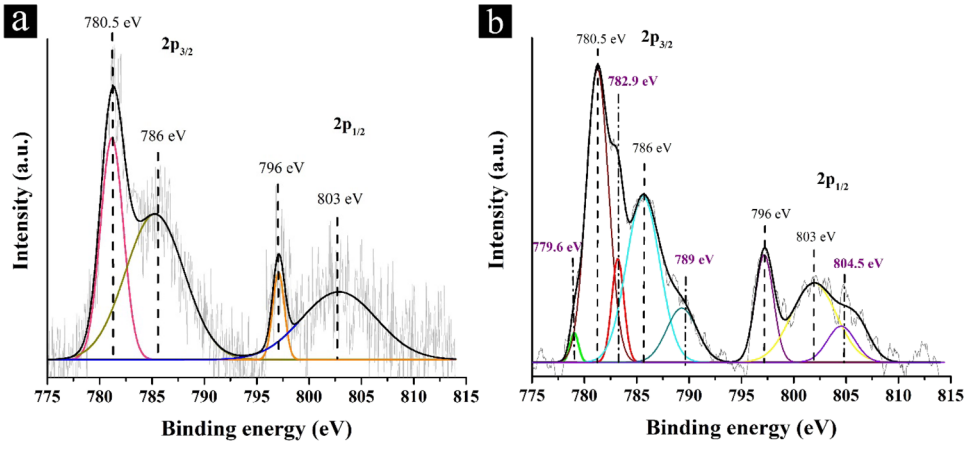

Figure 2. XPS spectra of the Co 2p peaks for (a) TMU-10 and (b) QT-300 samples and their best deconvolution to individual components.

https://doi.org/10.1021/acs.jpcc.1c08658
J. Phys. Chem. C 2022, 126, 683−692

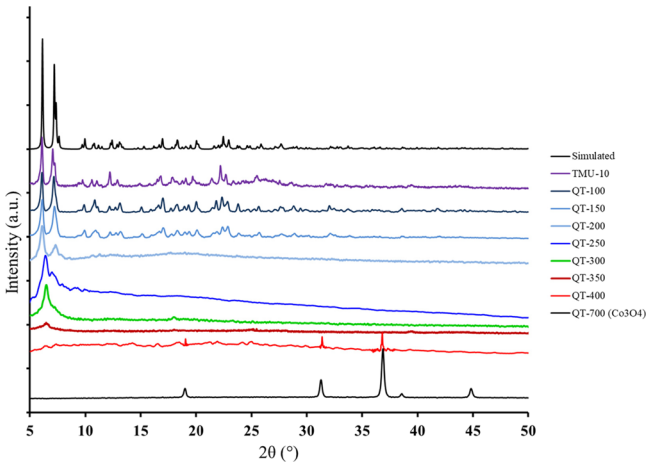

Figure 3. Comparison of PXRD patterns for simulated TMU-10, TMU-10, and QT-x.

ing also to Co_3O_4 according to XRD was also prepared to ensure the complete decomposition of the organic ligand.

The N_2 adsorption data collected at 77 K for TMU-10 and QT-300 revealed that the Brunauer–Emmett–Teller surface area, total pore volume, and total mesopore volume rise from 8.2 m^2/g, 0.023 cm^3/g, and 0.019 cm^3/g for TMU-10 to 38.8 m^2/g, 0.157 cm^3/g, and 0.142 cm^3/g for QT-300, respectively (Figure 4 and Table S1). Also, significant growth in the adsorption at high relative pressures ($P/P_0 > 0.9$) denotes the existence of large cavities. These observations can be related to partial deligandation of the TMU-10 and creating additional pores in the quasi MOF, QT-300. The Barrett–Joyner–Halenda pore size distribution also confirms the growth of the pore width in QT-300 generated by thermal treatment (Figure 4). Hence, the structural modifications triggered by the thermal treatment of TMU-10 lead to the generation of both micro and mesopores. This higher porosity, as well as the presence of coordinatively unsaturated Co sites, could influence the effective improvement of the catalytic activity of QT-300 compared to TMU-10.[30,41,42]

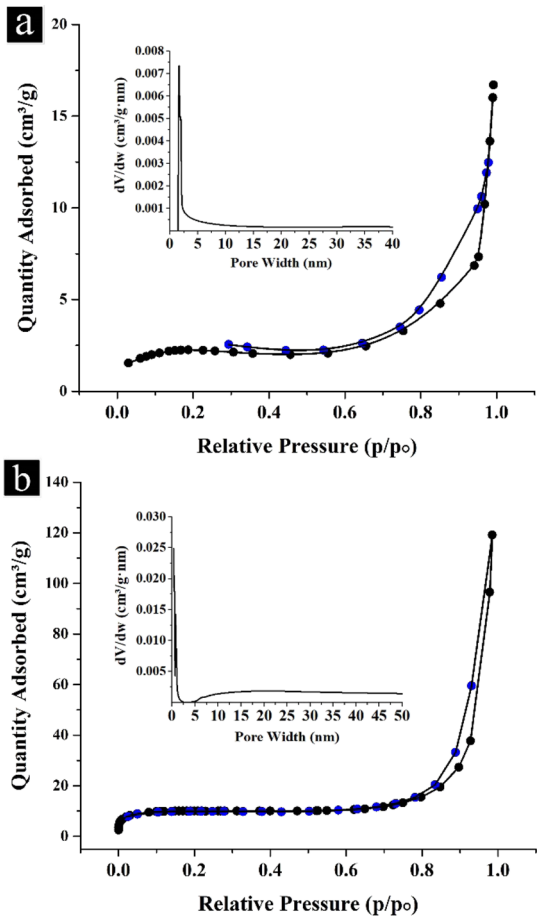

Figure 4. N_2 isotherm at 77 K and 1 bar and pore size distribution (insets) for (a) TMU-10 and (b) QT-300.

Transmission electron microscopy (TEM) images were obtained using Ga^+ to cut a slice of QT-300 thin enough to enable electron transmission. TEM images of QT-300 show internal cavities within the QT-300 crystals and the nucleation of very fine CoOx nanoparticles on the external part of the crystallite (Figure 5). These two characteristics are attributed to the effect of partial thermal deligandation of the TMU-10 structure.

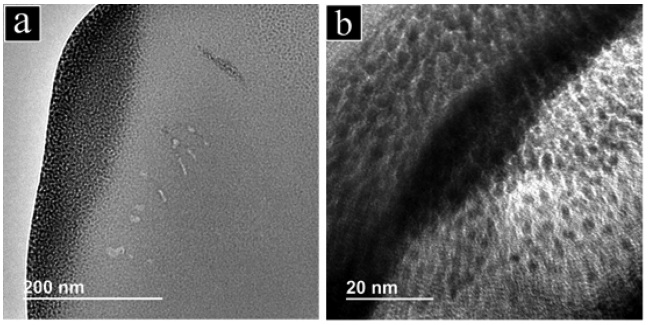

Figure 5. TEM images at two different magnifications taken upon cutting a thin slice of QT-300 with Ga^+-FIB, showing holes inside the lamella (a) and formation of very small CoOx nanoparticles in the outermost part of the QT-300 particle (b).

3.2. Catalytic 4-NP Reduction. To evaluate the activity of the QT-x samples as catalysts for the $NaBH_4$ reduction of 4-NP to 4-AP, the influence of the different factors was examined, including deligandation temperatures, comparison of the activity of the parent TMU-10 and obtained Co_3O_4 oxide, reaction temperature, and amount of catalyst. The kinetics of $NaBH_4$ reduction, including activation energy and adsorption enthalpy and entropy values in the presence of the most active catalyst, were also determined.

The strong UV absorption peak of 4-NP appearing at 317 nm shifts immediately to 400 nm upon addition of $NaBH_4$ which is related to the formation of 4-nitrophenolate ions. In a preliminary control in the absence of catalyst, no conversion of 4-NP in the presence of $NaBH_4$ was observed even after 24 h. In the presence of a suitable catalyst, the intensity of the absorption band corresponding to the anionic form of 4-NP at 400 nm gradually decreases along with the reaction time. The decrease at 400 nm is accompanied by a concomitant increase of a new peak at 300 nm corresponding to the formation of 4-AP (Figure S5). Visually, the bright yellow solution because of the basic form of 4-NP became colorless after its complete reduction of 4-NP.

3.3. Influence of TMU-10 Thermal Treatment Temperature. In the first place, the effect of deligandation temperature on the catalytic efficiencies of the quasi-MOFs,

https://doi.org/10.1021/acs.jpcc.1c08658
J. Phys. Chem. C 2022, 126, 683–692

that is, QT-100, QT-150, QT-200, QT-250, QT-300, QT-350, and QT-400 for the reduction of 4-NP at room temperature was evaluated (Table 1 and Figure 6). After addition of QT-x

Table 1. Effect of Deligandation Temperature on the Catalytic Activity of Quasi-MOFs for 4-NP Reduction[a]

quasi MOF	reduction time (min)	reduction (%)	induction period (s)
QT-100	180	17.1	150
QT-150	150	40	120
QT-200	120	80	60
QT-250	60	95	45
QT-300	2.5	99.7	20
QT-350	360	15	210
QT-400	360	33.8	170
QT-700[b]	360	34.5	180

[a]Experimental conditions: Catalyst mass = 1.0 mg, [4-NP] = 0.05 mM, [$NaBH_4$] = 10 mM, and T = 25 °C. [b]Co_3O_4.

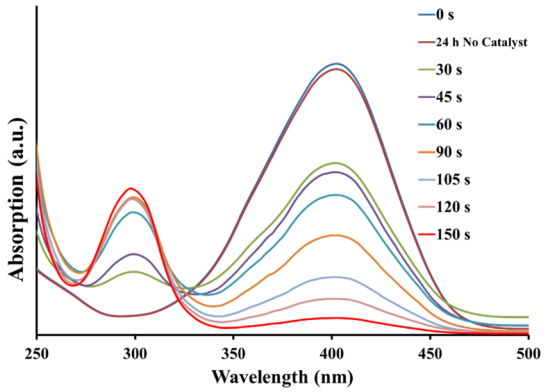

Figure 6. UV−vis spectra recorded at the indicated times for a 4-NP and $NaBH_4$ solution after adding the 1.0 mg QT-300 catalyst.

catalysts, the peak at 400 nm sharply decreased, eventually disappearing once the reaction was complete. At the same time, a new peak appeared at 300 nm, indicating the transformation of 4-NP into 4-AP. Two isosbestic points at 280 and 314 nm were observed, indicating that no side reactions take place (Figure 6).[10,43] Depending on the deligandation temperature, both the pore structure and the distribution of Co active sites change, and these factors affect the catalytic performance of the material.

According to PXRD up to 250 °C, the pore structure of TMU-10 remains intact with a minor defect generation, meaning a lower concentration of open cobalt sites. This is reflected in a moderate enhancement of the catalytic activity. Upon increasing the treatment temperature up to 300 °C, the catalytic activity was enhanced notably, diminishing the time needed to complete the reaction. The reduction performance was drastically reduced from 350 to 700 °C. The lowest catalytic activity was observed over QT-350. In contrast, the best reduction performance was observed in the presence of the QT-300 catalyst within 2.5 min. These observations can be explained based on thermogravimetric analysis (TGA), XPS, and XRD data. At a deligandation temperature of 150 °C, the Co(3) center in the framework loses a coordinated H_2O molecule and a coordination position vacancy on the cobalt increases the catalytic activity compared to QT-100. In the case of the QT-200 sample, there are two unsaturated cobalt centers of Co(3) (coordination number, C.N = 5) and Co(2) because of loss of two coordinated DMF molecules (C.N = 4). OH ligand bridging between three cobalt centers, Co(1), Co(2), and Co(3), in QT-250 is partially removed which leads to an enhanced catalytic performance up to 250 °C deligandation temperature. The complete removal of the OH bridge ligand occurs over the QT-300 catalyst, and its notable high activity is probably reflecting the synergistic effects of unsaturated cobalt sites originated from the conversion of a portion of Co(II) centers to Co(III) as well as generation of Co(II) in tetrahedral sites and the appearance of hierarchical meso and micropores (in accordance with type I and IV curves) in the catalyst. Thus, partial deligandation in the TMU-10 would create mesopores that would facilitate 4-NP uptake via π-π stacking interaction with the benzene ring increasing catalytic efficiency.

At higher deligandation temperatures, a major part of the QT-350 framework collapses, which dramatically reduces the observed catalytic activity. As the temperature increases, the Co_3O_4 phase appears which is responsible for 4-NP reduction in the QT-400 sample.

Also, the induction period, (t_0) in which no reduction reaction occurs, decreases from 150 to 20 s in the presence of TMU-10 and QT-300 catalysts, respectively, but increases afterward. The induction time is ascribed to reagent diffusion inside the pores and rebuilding of the catalyst surface by the reactants. This induction period is particularly notable in MOFs with structurally flexible lattices that have to adopt an open configuration before the reaction starts.[10] As a result, the reconstruction of the catalyst surface in the presence of QT-300 appears to be easier. According to the above description, the QT-300 sample is chosen as the best catalyst and is subsequently employed in the further experimental reduction reactions.

The amount and types of Lewis acid sites in TMU-10 parent and QT-300 catalysts were also estimated using NH_3-temperature-programmed desorption (TPD) (Figure S6 and Table S2). TMU-10 shows two NH_3 desorbed peaks at 174 and 313 °C that are related to low and medium acidity strength, respectively. For QT-300, these peaks showed up at 174 and 331 °C. TPD results indicate that QT-300 adsorbed a much higher NH_3 amount in comparison with its parent (TMU-10). In particular, partial deligandation of the pristine MOF at 300 °C results in an increase in total active acid sites by a factor of about 3 most of which is associated with the increase in medium acid sites. This increase in the strength and number of Lewis acid sites explains why the QT-300 catalyst exhibits higher catalytic activity in 4-NP reduction.

3.4. Effect of QT-300 Catalyst Dosage. Because the catalyst dosage is an important parameter in catalytic reduction, the effect of various amounts of QT-300 on the room-temperature reduction of 4-NP was also evaluated (Table 3 and Figure S7). In the absence of a catalyst, no detectable 4-NP conversion takes place for a long period. As summarized in Table 2, the reaction rate of 4-NP reduction increases with the amount of QT-300. Thus, 4-NP conversion reaches 99.2% within 3 min over 0.1 mg of the QT-300 catalyst. As the amount of the QT-300 catalyst increased further up to 1.0 mg, 4-NP conversion reached somewhat higher conversion in a shorter reaction time. In view of the results shown in Table 2, 0.1 mg was chosen as the suitable QT-300 amount in subsequent experiments.

3.5. Reaction Kinetics. Because the amount of $NaBH_4$ considerably exceeds that of 4-NP in the solution, the catalytic

https://doi.org/10.1021/acs.jpcc.1c08658
J. Phys. Chem. C 2022, 126, 683−692

Table 2. Effect of the QT-300 Amount as a Catalyst in Reduction of 4-NP[a]

entry	catalyst dosage (mg)	reduction (%)	reduction time[b] (min)	4-AP yield[c] (%)
1	0	0	a week	0
2	0.05	80	30	67
3	0.1	99.2	3	87
4	0.2	99.3	3	88.5
5	0.5	99.5	3	90
6	1.0	99.7	2.5	91.5

[a]Experimental conditions: [4-NP] = 0.05 mM, [$NaBH_4$] = 10 mM at RT. [b]Reduction time = Time after subtraction of the induction period, t_0, for each catalytic run. [c]Yield is related to 4-AP concentration changes in λ_{max} = 300 nm.

reduction reaction could be considered as obeying pseudofirst-order kinetics with regard to the 4-NP concentration. As observed in Figure S8, the plots of $\ln(C/C_0)$ versus reaction time for the reduction of 4-NP using QT-300 and TMU-10 catalysts follows a linear relationship with reaction time. The pseudofirst-order rate constant values (k_{app}) at for TMU-10 and QT-300 catalysts were 1.0×10^{-4} s^{-1} and 2.8×10^{-2} s^{-1}, respectively. Thus, the QT-300 catalyst exhibits an about 282 times higher activity factor than the TMU-10 catalyst (Table 3). Also, the half-life time of the catalytic reduction decreases

Table 3. Comparison of Apparent Reaction Rate (k), Half-Life ($t_{1/2}$), and Relative Activity Factor Values (K) for TMU-10 and QT-300 Catalysts in the Room-Temperature Reduction of 4-NP[a]

catalyst	k_{app} (s^{-1})	$t_{1/2}$ (s)	K (s^{-1} g^{-1})
TMU-10	1.0×10^{-4}	7000	1
QT-300	2.82×10^{-2}	24.8	282

[a]Experimental conditions: [4-NP] = 0.05 mM, [$NaBH_4$] = 10 mM, catalyst mass = 0.1 mg at RT.

from 116.6 min to 24.8 s in the presence of TMU-10 and QT-300 catalysts, respectively. The different activity between them can be attributed to the greater density of active sites and easier diffusion to the active sites with a much more favorable pore distribution for QT-300. Thus, the synergistic effects of two unsaturated cobalt centers (Co(III) and Co(II) in tetrahedral sites) and simultaneous existence of both meso and micropores in the catalyst are probably responsible for better adsorption of 4-NP and BH_4^- ions and the decrease in the apparent kinetic barrier, resulting in the superior catalytic performance of QT-300 compared to its parent (TMU-10). The turnover frequency (TOF) of the QT-300 catalyst, defined as the number of moles of 4-NP converted by per mole of Co in the catalyst per second, is 0.02 s^{-1}.

3.6. Comparison of the Catalytic Performance of TMU-10, QT-300, and Co_3O_4. The catalytic activity of QT-300, the best catalyst obtained by thermal treatment, was compared with that of its parent precursor (TMU-10) and residual metal oxide (Co_3O_4). As shown in Table 1, the catalytic conversion of 4-NP to 4-AP in the presence of the QT-300 catalyst occurs at about 5.8 and 3.3 times faster than in the presence of TMU-10 and Co_3O_4, respectively. In principle, 4-nitrophenolate and BH_4^-, being both negative ions, should undergo Coulombic repulsion disfavoring their reaction. The presence of a large number of unsaturated metal nodes across the framework of the QT-300 catalyst can significantly favor adsorb these negative ions onto the coordinatively unsaturated position of the positive Co sites, thus diminishing the reaction kinetic barrier and reacting in a much shorter time with much higher efficiency. Additionally, electron transfer in this defective material resulting in the formation of hydride species from borohydride should be easier.[43] In the cases of TMU-10 and Co_3O_4, the lack of unsaturated positions and the impeded accessibility to the active sites should be factors increasing the kinetic energy barrier.

3.7. Mechanistic Studies. Understanding the reaction mechanism can assist in designing a better catalyst with improved progress and efficiency. Most heterogeneous catalytic reactions occur through either Eley–Rideal (ER) or Langmuir–Hinshelwood (LH) pathways.[10,44] In the ER model, only one of the reactants will be adsorbed on the catalyst surface and react with the other reactant in the solution, while the LH model implies the adsorption of both reagents on the catalyst surface.

In the case of 4-NP reduction over QT-300, these two general mechanisms can be distinguished by investigating the rate-constant dependence on the concentration of 4-NP and $NaBH_4$. In ER model, the rate constant should increase with an increasing concentration of 4-NP because this reagent is not adsorbed on the catalyst surface. According to the LH model, the rate constant should decrease with an increasing concentration of 4-NP, whereas for an increasing concentration of $NaBH_4$, the reaction rate would reach a maximum.[9,44,45] In addition, the apparent rate constant is proportional to the surface area of the catalyst (S). The kinetic constants can be calculated as:

$$\frac{dc_{NP}}{dt} = -k_{app}c_{NP} = -k_1 S c_{NP} \quad (5)$$

For the quantitative comparison of the data, the catalytic reduction can be modeled by the Langmuir–Freundlich isotherm:

$$\Theta_i = \frac{(K_i c_i)^{n_i}}{1 + \sum_{j=1}^{N} (K_j c_j)} \quad (6)$$

where θ_i is the surface coverage of the compound i, K_i is the adsorption constant of the respective component, and c_i is the concentration in solution and 'n' is related to the heterogeneity of the sorbent. Further rearrangement of eq 5 creates eq 7 which can be applied to model the catalytic activity.

$$-\frac{dc_{NP}}{dt} = \frac{kS(K_{NP}c_{NP})^n (K_{BH_4}c_{BH_4})^m}{(1 + (K_{NP}c_{NP})^n + (K_{BH_4}c_{BH_4})^m)^2} = k_{app}c_{NP} \quad (7)$$

Thus, k_{app} is calculated by:

$$k_{app} = \frac{kSK_{NP}^n c_{NP}^{n-1} (K_{BH_4}c_{BH_4})^m}{(1 + (K_{NP}c_{NP})^n + (K_{BH_4}c_{BH_4})^m)^2} \quad (7a)$$

where, k is the molar rate constant per square meter of the catalyst and K_{NP} and K_{BH4} are the adsorption constants of 4-NP and BH_4^-, respectively.

Figure 7 presents the nonlinear dependence of rate constant as a function of both 4-NP and $NaBH_4$ concentration. The solid lines refer to the fit of the experimental data to eq 7a, suggesting that the present catalytic reaction follows the LH

https://doi.org/10.1021/acs.jpcc.1c08658
J. Phys. Chem. C 2022, 126, 683–692

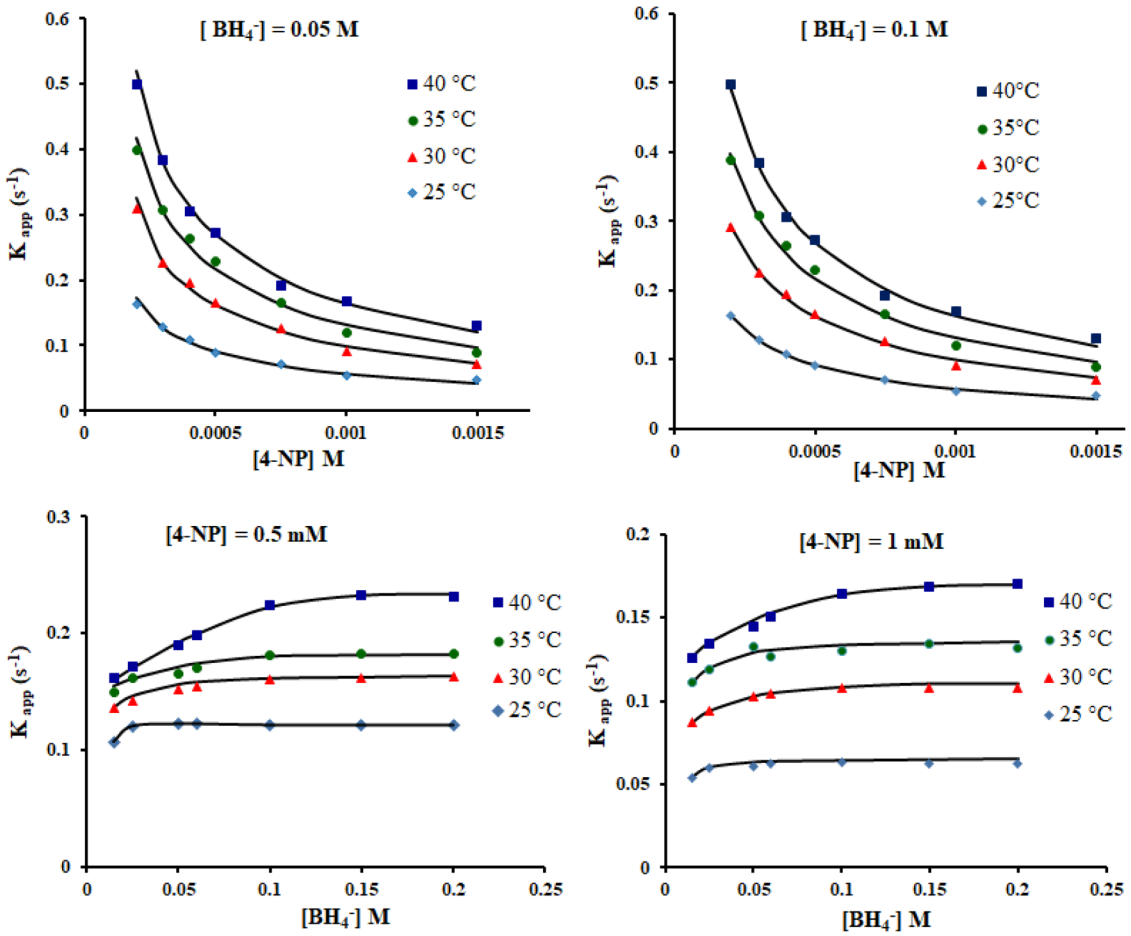

Figure 7. Dependence of the apparent rate constant (k_{app}) on 4-NP and BH_4^- concentrations at various temperatures. The black solid lines are the fit of the L-H model with the calculated surface area of the QT-300 catalyst in solution of 0.1552 m^2 L^{-1}.

model. All the parameters related to these fits are summarized in Table 4. By increasing the temperature, K_{NP} increases while

Table 4. Rate and Adsorption Constants of 4-NP and BH_4^- over the QT-300 Catalyst at Different Temperatures, Obtained by Fitting the Experimental Data to the LH Model According to eq 7a[a]

temperature (°K)	k [mol/m^2 s]	K_{NP} [L/mol]	K_{BH_4} [L/mol]
298	$(2.9 \pm 0.1) \times 10^{-3}$	1323 ± 118	50 ± 14
303	$(4.5 \pm 0.1) \times 10^{-3}$	1940 ± 170	51 ± 15
308	$(5.7 \pm 0.1) \times 10^{-3}$	2544 ± 225	56 ± 16
313	$(6.9 \pm 0.1) \times 10^{-3}$	3176 ± 285	63 ± 18

[a] n = 0.5 and m = 1 Freundlich exponents in eq 7a.

$K_{BH_4^-}$ is almost the same in the temperature range of 25−40 °C. These results suggest that first, 4-NP is quickly reduced to the 4-hydroxylaminophenol intermediate, and then it is slowly reduced to the final 4-AP product. In other words, the second step ($K_{BH_4^-}$) is the rate-determining step.

Here, the rate constant decreases with increasing concentrations of 4-NP and increases with increasing concentrations of $NaBH_4$. Obviously there is a competition between both reactants for active Co sites on the QT-300 surface. The diffusion of the reactants to the unsaturated Co surfaces of the QT-300 catalyst and the adsorption/desorption equilibrium is surmised to be fast. In the rate-determining step, the surface hydrogen and 4-NP react with each other and the 4-AP is desorbed from the surface of the QT-300 catalyst. Separation of the 4-AP product releases a free catalytic surface and catalytic turn over can begin again. A high concentration of 4-NP causes the full coverage of the catalytic surface which slowly decreases the catalytic activity. Increasing the concentration of $NaBH_4$ leads to an increase in the rate constant. Further increase in the $NaBH_4$ concentration causes the maximum rate constant because of the site saturation on the catalyst surface. According to the results, both BH_4^- ions and 4-NP simultaneously adsorb on the surface of the QT-300 catalyst, and then the 4-AP product is desorbed out (Scheme 1).

Thermodynamic parameters for the heterogeneous catalytic reduction of 4-NP over the QT-300 catalyst were determined by performing the reduction at different temperatures (25−40 °C) and obtaining the true (k) rate constant at each temperature. The true activation energy ($E_{A,k}$) was calculated at about 44 kJ/mol by the Arrhenius equation:

$$\mathrm{Ln}(k) = \ln A - \frac{E_A}{RT} \tag{8}$$

The activation parameters including activation enthalpy ($\Delta H^{\#}$) and activation entropy ($\Delta S^{\#}$) were also estimated by the Eyring equation for both reactants:

https://doi.org/10.1021/acs.jpcc.1c08658
J. Phys. Chem. C 2022, 126, 683−692

Scheme 1. Illustration of the LH Mechanism for the Reduction of 4-NP by $NaBH_4^-$ Promoted by the QT-300 Catalyst

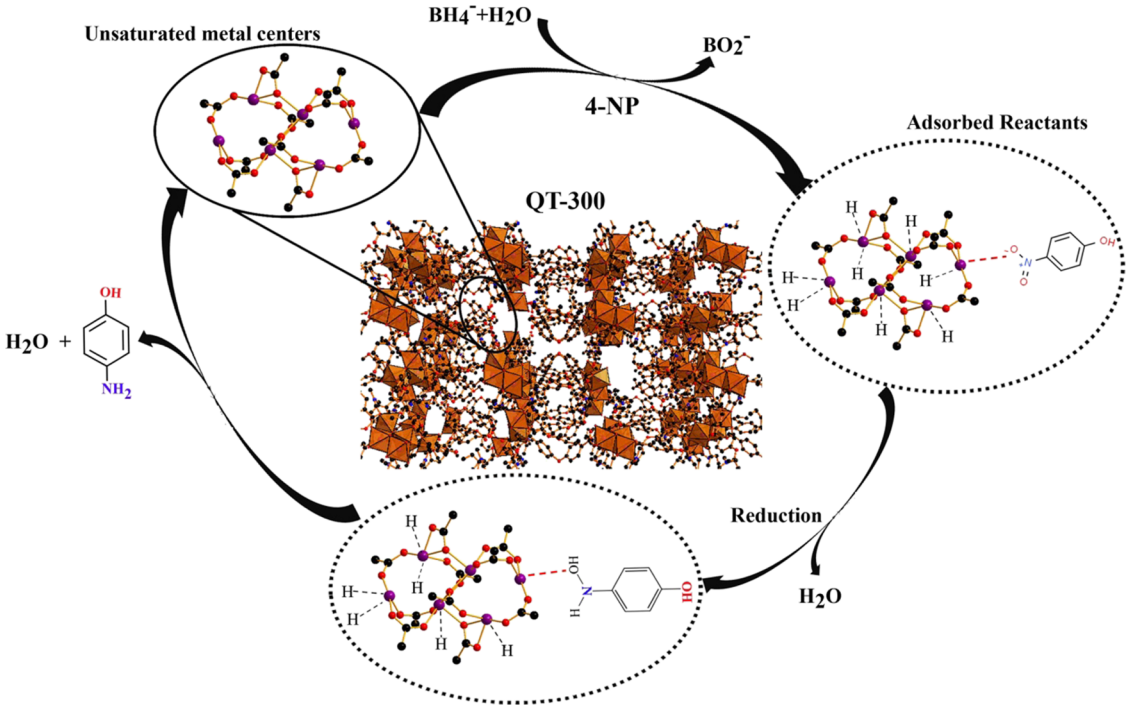

$$\ln\left(\frac{k}{T}\right) = -\frac{\Delta H^{\#}}{RT} + \frac{\Delta S^{\#}}{R} \quad (9)$$

Then Gibbs free-energy of activation $\Delta G^{\#}$ at 25 °C was also calculated. As presented in Table 5, the adsorption process for 4-NP molecules is endothermic with a positive value of activation entropy, indicating the release of water molecules and/or other species bonded to the catalyst surface. The negative $\Delta G^{\#}_{298}$ value for 4-NP indicates that the reaction occurs spontaneously over this reactant. Also, in the case of $NaBH_4$, the $\Delta G^{\#}_{298}$ value is positive showing that the catalytic conversion is feasible over the QT-300 catalyst at room temperature which is consistent with the experimental observations. The activity factor of the QT-300 catalyst indicates that QT-300 is able to compete favorably with other reported cobalt-based catalysts (Table 6). Although comparison of the performance of various catalysts reported in different laboratories is always problematic, the large $NaBH_4$ excess used in all the studies to make pseudofirst-order the reduction reaction that was carried out at ambient temperature allows using the apparent first-order rate constant (k_{app}) and the apparent activity as quantitative values of the relative catalytic activity to rank catalyst performance.

Table 5. Activation Parameters of the Adsorption Process of 4-NP and BH_4 on the Surface of the QT-300 Catalyst

parameters	K_{4-NP}	k_{BH4^-}
$\Delta H^{\#}$ (kJ/mol)	42.5 ± 0.2	9.6 ± 0.1
$\Delta S^{\#}$ (J/mol K)	155.3 ± 0.8	17.2 ± 2.4
$\Delta G^{\#}_{298}$ (kJ/mol)	−3.8 ± 0.1	4.5 ± 0.6

3.8. Reusability of the QT-300 Catalyst. To examine the reusability of the catalyst, the reduction of 4-NP was carried out for five catalytic runs using the same QT-300 sample. Conversion values remained relatively unchanged even after the fifth catalytic run (Figure S9a). In addition, no changes in the XRD pattern of the QT-300 sample after five reuses was observed (Figure S9b), indicating the structural stability of the catalyst. Moreover, inductively coupled plasma measurements did not reveal a significant amount of cobalt in the supernatant after each cycle, showing that no leaching of the catalyst into the aqueous media happens. These results indicate that the structure and catalytic activity of QT-300 remain stable under reaction conditions in the reduction of 4-NP.

Table 6. Comparison of the Activity Factor of QT-300 with Other Reported Cobalt-Based Catalysts for the Conversion of 4-NP to 4-AP at Room Temperature

catalysts	$NaBH_4$ (mol)/4-NP (mol)	k_{app} (s^{-1})	K (s^{-1} g^{-1})	E_a (kJ/mol)	reference
NRGO-$CoWO_4$-Fe_2O_3	111	8.4×10^{-2}	84		46
$CoWO_4$-Fe_2O_3	111	3.6×10^{-2}	36		46
Au/$CoFe_2O_4$	-	4.4×10^{-3}	44		47
Co_3O_4	600	3.0×10^{-3}	60		48
MOF-derived nickel−cobalt bimetal oxide (Ni-Co-O)	600	1.0×10^{-2}	200		48
5.1 wt % Co-doped CuO NPs	67	43.8	43.8		49
QT-300	200	2.8×10^{-2}	282	44	this study

https://doi.org/10.1021/acs.jpcc.1c08658
J. Phys. Chem. C 2022, 126, 683−692

4. CONCLUSIONS

Postsynthetic defect engineering on a cobalt-based metal−organic framework, $[Co_6(oba)_5(OH)_2(H_2O)_2(DMF)_4]_n \cdot 2DMF$, can be conveniently carried out via regulated thermal processing in an air atmosphere at diverse temperatures in the range of 100−700 °C. The quasi TMU-10 calcined at 300 °C showed best catalytic performance with an apparent rate constant, activity factor, and half-life time of 2.8×10^{-2} s^{-1}, 282 s^{-1} g^{-1}, and 24.8 s, respectively. The synergistic effects between the uniform distribution of higher density and strength of Lewis acid sites on cobalt nodes and the generation of micro and mesopores (types I and IV) are the two main factors responsible for this enhanced catalytic performance that is over five times that of the parent TMU-10. Mechanism studies indicate that the reduction of 4-NP follows the LH model, and the attack of 4-NP by the surface-attached hydrogen species is the rate-determining step. Thus, the present study shows that going beyond generation of defects, a deeper partial destruction of the MOF structure appears as a general, economic, and green method to obtain advanced catalysts with application in the removal of organic pollutants from contaminated waste water and even inorganic cations by incorporation into the QT-x framework.[50]

■ ASSOCIATED CONTENT

Supporting Information

The Supporting Information is available free of charge at https://pubs.acs.org/doi/10.1021/acs.jpcc.1c08658.

PXRD patterns, FESEM images, TGA profiles, and Fourier transform infrared spectra (PDF)

■ AUTHOR INFORMATION

Corresponding Authors

Mohammad Yaser Masoomi − *Department of Chemistry, Faculty of Science, Arak University, Arak 3848177584, Iran*; Email: m-masoomi@araku.ac.ir

Hermenegildo García − *Instituto de Tecnología Química, Universitat Politecnica de Valencia-Consejo Superior de Investigaciones Científicas, Universitat Politecnica de Valencia, Valencia 46022, Spain*; orcid.org/0000-0002-9664-493X; Email: hgarcia@upv.es

Authors

Minoo Bagheri − *Department of Chemistry, Faculty of Science, Arak University, Arak 3848177584, Iran*

Amparo Forneli − *Instituto de Tecnología Química, Universitat Politecnica de Valencia-Consejo Superior de Investigaciones Científicas, Universitat Politecnica de Valencia, Valencia 46022, Spain*

Complete contact information is available at: https://pubs.acs.org/10.1021/acs.jpcc.1c08658

Notes

The authors declare no competing financial interest.

■ ACKNOWLEDGMENTS

This work was supported by Iran Science Elites Federation and Arak University.

■ REFERENCES

(1) Din, M. I.; Khalid, R.; Hussain, Z.; Hussain, T.; Mujahid, A.; Najeeb, J.; Izhar, F. Nanocatalytic Assemblies for Catalytic Reduction of Nitrophenols: A Critical Review. *Crit. Rev. Anal. Chem.* **2020**, *50*, 322−338.

(2) Strachan, J.; Barnett, C.; Masters, A. F.; Maschmeyer, T. 4-Nitrophenol Reduction: Probing the Putative Mechanism of the Model Reaction. *ACS Catal.* **2020**, *10*, 5516−5521.

(3) Zhao, H.; Li, Y.; Wang, D.; Zhao, L. Synthesis of N-Doped Core−Shell-Structured Porous CoSe@C Composites and their Efficient Catalytic Activity for the Reduction of 4-Nitrophenol. *Eur. J. Inorg. Chem.* **2018**, *2018*, 1145−1151.

(4) Sun, J.; Fu, Y.; He, G.; Sun, X.; Wang, X. Catalytic hydrogenation of nitrophenols and nitrotoluenes over a palladium/graphene nanocomposite. *Catal. Sci. Tech.* **2014**, *4*, 1742−1748.

(5) Gupta, V. K.; Atar, N.; Yola, M. L.; Üstündağ, Z.; Uzun, L. A novel magnetic Fe@Au core−shell nanoparticles anchored graphene oxide recyclable nanocatalyst for the reduction of nitrophenol compounds. *Water Res.* **2014**, *48*, 210−217.

(6) Ghosh, B. K.; Moitra, D.; Chandel, M.; Patra, M. K.; Vadera, S. R.; Ghosh, N. N. CuO Nanoparticle Immobilised Mesoporous TiO_2−Cobalt Ferrite Nanocatalyst: A Versatile, Magnetically Separable and Reusable Catalyst. *Catal. Lett.* **2017**, *147*, 1061−1076.

(7) Jiang, H.-L.; Akita, T.; Ishida, T.; Haruta, M.; Xu, Q. Synergistic Catalysis of Au@Ag Core−Shell Nanoparticles Stabilized on Metal−Organic Framework. *J. Am. Chem. Soc.* **2011**, *133*, 1304−1306.

(8) Chang, Y.-C.; Chen, D.-H. Catalytic reduction of 4-nitrophenol by magnetically recoverable Au nanocatalyst. *J. Hazard. Mater.* **2009**, *165*, 664−669.

(9) Wunder, S.; Polzer, F.; Lu, Y.; Mei, Y.; Ballauff, M. Kinetic Analysis of Catalytic Reduction of 4-Nitrophenol by Metallic Nanoparticles Immobilized in Spherical Polyelectrolyte Brushes. *J. Phys. Chem. C* **2010**, *114*, 8814−8820.

(10) Wunder, S.; Lu, Y.; Albrecht, M.; Ballauff, M. Catalytic Activity of Faceted Gold Nanoparticles Studied by a Model Reaction: Evidence for Substrate-Induced Surface Restructuring. *ACS Catal.* **2011**, *1*, 908−916.

(11) Hu, M.; Zhang, Z.; Luo, C.; Qiao, X. One-Pot Green Synthesis of Ag-Decorated SnO_2 Microsphere: an Efficient and Reusable Catalyst for Reduction of 4-Nitrophenol. *Nanoscale Res. Lett.* **2017**, *12*, 435.

(12) Xu, G.-W.; Wu, Y.-P.; Dong, W.-W.; Zhao, J.; Wu, X.-Q.; Li, D.-S.; Zhang, Q. A Multifunctional Tb-MOF for Highly Discriminative Sensing of Eu^{3+}/Dy^{3+} and as a Catalyst Support of Ag Nanoparticles. *Small* **2017**, *13*, No. 1602996.

(13) Liu, Y.; Wang, S.; Yu, B.; Zhang, Y.; Kong, X.; Mi, Y.; Zhang, J.; Guo, Z.; Xu, W.; Chen, X. Progressive Increasing of Pt Nanoparticles with Multiple-Layered Manner inside Metal−Organic Frameworks for Enhanced Catalytic Activity. *Inorg. Chem.* **2020**, *59*, 13184−13189.

(14) Mogudi, B. M.; Ncube, P.; Bingwa, N.; Mawila, N.; Mathebula, S.; Meijboom, R. Promotion effects of alkali- and alkaline earth metals on catalytic activity of mesoporous Co3O4 for 4-nitrophenol reduction. *Appl. Catal., B* **2017**, *218*, 240−248.

(15) Sahiner, N.; Ozay, H.; Ozay, O.; Aktas, N. A soft hydrogel reactor for cobalt nanoparticle preparation and use in the reduction of nitrophenols. *Appl. Catal., B* **2010**, *101*, 137−143.

(16) Corma, A.; García, H.; Llabrés i Xamena, F. X. Engineering Metal Organic Frameworks for Heterogeneous Catalysis. *Chem. Rev.* **2010**, *110*, 4606−4655.

(17) Dhakshinamoorthy, A.; Li, Z.; Garcia, H. Catalysis and photocatalysis by metal organic frameworks. *Chem. Soc. Rev.* **2018**, *47*, 8134−8172.

(18) Dhakshinamoorthy, A.; Asiri, A. M.; García, H. Metal−Organic Framework (MOF) Compounds: Photocatalysts for Redox Reactions and Solar Fuel Production. *Chemistry (Weinheim an der Bergstrasse, Germany)* **2016**, *55*, 5414−5445.

(19) Alvaro, M.; Carbonell, E.; Ferrer, B.; Llabrés i Xamena, F. X.; Garcia, H. Semiconductor Behavior of a Metal-Organic Framework (MOF). *Chem. − Eur. J.* **2007**, *13*, 5106−5112.

(20) Jin, Z.; Li, Y.; Ma, Q. CoAl LDH@Ni-MOF-74 S-Scheme Heterojunction for Efficient Hydrogen Evolution. *Trans. Tianjin Univ.* **2021**, *27*, 127−138.

(21) Qin, Y.; Guo, J.; Zhao, M. Metal−Organic Framework-Based Solid Acid Materials for Biomass Upgrade. *Trans. Tianjin Univ.* **2021**, *27*, 434−449.
(22) Masoomi, M. Y.; Bagheri, M.; Morsali, A. Enhancement of photocatalytic performance in two zinc-based metal-organic frameworks by solvent assisted linker exchange. *CrystEngComm* **2017**, *19*, 5749−5754.
(23) Masoomi, M. Y.; Bagheri, M.; Morsali, A. Application of Two Cobalt-Based Metal−Organic Frameworks as Oxidative Desulfurization Catalysts. *Inorg. Chem.* **2015**, *54*, 11269−11275.
(24) Doonan, C. J.; Sumby, C. J. Metal−organic framework catalysis. *CrystEngComm* **2017**, *19*, 4044−4048.
(25) Dhakshinamoorthy, A.; Garcia, H. Catalysis by metal nanoparticles embedded on metal−organic frameworks. *Chem. Soc. Rev.* **2012**, *41*, 5262−5284.
(26) Kim, J.; Kim, S.-N.; Jang, H.-G.; Seo, G.; Ahn, W.-S. CO_2 cycloaddition of styrene oxide over MOF catalysts. *Appl. Catal., A* **2013**, *453*, 175−180.
(27) Bagheri, M.; Masoomi, M. Y.; Morsali, A. High organic sulfur removal performance of a cobalt based metal-organic framework. *J. Hazard. Mater.* **2017**, *331*, 142−149.
(28) Shen, Y.; Bao, L.-W.; Sun, F.-Z.; Hu, T.-L. A novel Cu-nanowire@Quasi-MOF via mild pyrolysis of a bimetal-MOF for the selective oxidation of benzyl alcohol in air. *Mater. Chem. Front* **2019**, *3*, 2363−2373.
(29) Fan, L.; Zhao, F.; Huang, Z.; Chen, B.; Zhou, S.-F.; Zhan, G. Partial deligandation of M/Ce-BTC nanorods (M = Au, Cu, au-cu) with "Quasi-MOF" structures towards improving catalytic activity and stability. *Appl. Catal., A* **2019**, *572*, 34−43.
(30) Tsumori, N.; Chen, L.; Wang, Q.; Zhu, Q.-L.; Kitta, M.; Xu, Q. Quasi-MOF: Exposing Inorganic Nodes to Guest Metal Nanoparticles for Drastically Enhanced Catalytic Activity. *Chem* **2018**, *4*, 845−856.
(31) Yang, H.; Peng, F.; Dang, C.; Wang, Y.; Hu, D.; Zhao, X.; Feng, P.; Bu, X. Ligand Charge Separation To Build Highly Stable Quasi-Isomer of MOF-74-Zn. *J. Am. Chem. Soc.* **2019**, *141*, 9808−9812.
(32) Dong, P.; Wang, H.; Liu, W.; Wang, S.; Wang, Y.; Zhang, J.; Lin, F.; Wang, Y.; Zhao, C.; Duan, X.; Wang, S.; Sun, H. Quasi-MOF derivative-based electrode for efficient electro-Fenton oxidation. *J. Hazard. Mater.* **2021**, *401*, No. 123423.
(33) Ryder, M. R.; Maul, J.; Civalleri, B.; Erba, A. Quasi-Harmonic Lattice Dynamics of a Prototypical Metal−Organic Framework. *Adv. Theory Simul.* **2019**, *2*, No. 1900093.
(34) Bagheri, M.; Masoomi, M. Y.; Domínguez, E.; García, H. High hydrogen release catalytic activity by quasi-MOFs prepared via post-synthetic pore engineering. *Sustainable Energy Fuels* **2021**, *5*, 4587−4596.
(35) Corma, A.; García, H. Lewis Acids as Catalysts in Oxidation Reactions: From Homogeneous to Heterogeneous Systems. *Chem. Rev.* **2002**, *102*, 3837−3892.
(36) Bagheri, M.; Melillo, A.; Ferrer, B.; Masoomi, M. Y.; Garcia, H. Enhanced Catalytic Performance of Quasi-HKUST-1 for the Tandem Imine Formation. *Chem. − Eur. J.* **2021**, *27*, 14273−14281.
(37) Bagheri, M.; Mahjoub, A. R. Template assisted fast photocatalytic degradation of azo dye using ferric oxide-gallia nanostructures. *RSC Adv.* **2016**, *6*, 87555−87563.
(38) Wen, Y.; Zhang, J.; Xu, Q.; Wu, X.-T.; Zhu, Q.-L. Pore surface engineering of metal−organic frameworks for heterogeneous catalysis. *Coord. Chem. Rev.* **2018**, *376*, 248−276.
(39) Liu, J.-X.; Su, Y.; Filot, I. A. W.; Hensen, E. J. M. A Linear Scaling Relation for CO Oxidation on CeO2-Supported Pd. *J. Am. Chem. Soc.* **2018**, *140*, 4580−4587.
(40) Chuang, T. J.; Brundle, C. R.; Rice, D. W. Interpretation of the x-ray photoemission spectra of cobalt oxides and cobalt oxide surfaces. *Surf. Sci.* **1976**, *59*, 413−429.
(41) Fantauzzi, M.; Secci, F.; Sanna Angotzi, M.; Passiu, C.; Cannas, C.; Rossi, A. Nanostructured spinel cobalt ferrites: Fe and Co chemical state, cation distribution and size effects by X-ray photoelectron spectroscopy. *RSC Adv.* **2019**, *9*, 19171−19179.
(42) Biesinger, M. C.; Payne, B. P.; Grosvenor, A. P.; Lau, L. W. M.; Gerson, A. R.; Smart, R. S. C. Resolving surface chemical states in XPS analysis of first row transition metals, oxides and hydroxides: Cr, Mn, Fe, Co and Ni. *Appl. Surf. Sci.* **2011**, *257*, 2717−2730.
(43) Huang, J.; Vongehr, S.; Tang, S.; Lu, H.; Meng, X. Highly Catalytic Pd−Ag Bimetallic Dendrites. *J. Phys. Chem. C* **2010**, *114*, 15005−15010.
(44) Aditya, T.; Pal, A.; Pal, T. Nitroarene reduction: a trusted model reaction to test nanoparticle catalysts. *Chem. Commun.* **2015**, *51*, 9410−9431.
(45) Gu, S.; Wunder, S.; Lu, Y.; Ballauff, M.; Fenger, R.; Rademann, K.; Jaquet, B.; Zaccone, A. Kinetic Analysis of the Catalytic Reduction of 4-Nitrophenol by Metallic Nanoparticles. *J. Phys. Chem. C* **2014**, *118*, 18618−18625.
(46) Mohamed, M. J. S.; Shenoy, U. S.; Bhat, D. K. Novel NRGO-$CoWO_4$-Fe_2O_3 nanocomposite as an efficient catalyst for dye degradation and reduction of 4-nitrophenol. *Mater. Chem. Phys.* **2018**, *208*, 112−122.
(47) Saire-Saire, S.; Barbosa, E. C.; Garcia, D.; Andrade, L. H.; Garcia-Segura, S.; Camargo, P. H.; Alarcon, H. Green synthesis of Au decorated $CoFe_2O_4$ nanoparticles for catalytic reduction of 4-nitrophenol and dimethylphenylsilane oxidation. *RSC Adv.* **2019**, *9*, 22116−22123.
(48) Khan, A.; Wei, D.; Wang, Z.; Su, X.; Wang, J.; Alam, S.; Wang, L.; Wu, R.; Maloletnev, A. S.; Yang, C. MOF-derived nickel−cobalt bimetal oxide nanostructures as a cooperative catalyst for the reduction of 4-nitrophenol. *J. Chem. Technol. Biotechnol.* **2021**, *96*, 697−703.
(49) Sharma, A.; Dutta, R. K.; Roychowdhury, A.; Das, D.; Goyal, A.; Kapoor, A. Cobalt doped CuO nanoparticles as a highly efficient heterogeneous catalyst for reduction of 4-nitrophenol to 4-aminophenol. *Appl. Catal., A* **2017**, *543*, 257−265.
(50) Chi, H.; Wang, J.; Wang, H.; Li, S.; Yang, M.; Bai, S.; Li, C.; Sun, X.; Zhao, Y.; Song, Y.-F. Super-Stable Mineralization of Ni^{2+} Ions from Wastewater using CaFe Layered Double Hydroxide. *Adv. Funct. Mater.* , 2106645, DOI: 10.1002/adfm.202106645.